Environ Earth Sci (2014) 71:3081–3094
DOI 10.1007/s12665-013-2684-5

ORIGINAL ARTICLE

High-resolution aquifer analog of fluvial–aeolian sediments of the Guarani aquifer system

Dominik Höyng · Fernando Mazo D'Affonseca · Peter Bayer · Edson Gomes de Oliveira · José Alexandre J. Perinotto · Fábio Reis · Holger Weiß · Peter Grathwohl

Received: 1 February 2013 / Accepted: 19 July 2013 / Published online: 6 August 2013

Abstract The Guarani aquifer system (GAS) represents one of the biggest aquifers in the world and is the most relevant groundwater resource in South America. For the first time, by combining field and laboratory measurements, a high-resolution aquifer analog model of fluvial–aeolian sediments of the GAS in São Paulo State (Brazil) is constructed. Three parallel sections of frontal outcrops, 28 m × 5.8 m, and two parallel sections of lateral outcrops, 7 m × 5.8 m, are recorded during open-pit mining of sandy sediments and describe in detail the three-dimensional distribution of the local lithofacies and hydrofacies. Variations of hydraulic conductivity, K, and porosity, n, are resolved on the centimeter scale, and the most permeable units of the fluvial–aeolian facies association are identified. The constructed aquifer analog model shows moderate hydraulic heterogeneity and a mean K value of 1.36×10^{-4} m/s, which is greater than the reported range of K values for the entire GAS in São Paulo State. The results suggest that the examined sedimentary unit constitutes a relevant portion of the GAS in São Paulo State in the context of groundwater extraction and pollution. Moreover, the constructed aquifer analog is considered an ideal basis for future numerical model experiments, aiming at in-depth understanding of the groundwater flow and contaminant transport patterns at this GAS portion or at comparable fluvial–aeolian facies associations.

Keywords Groundwater reservoir analog model · Guarani aquifer · Reservoir characterization · Fluvial–aeolian sediments · Pirambóia Formation

D. Höyng (✉) · F. M. D'Affonseca · P. Grathwohl
University of Tübingen, Center for Applied Geosciences, Hölderlinstr. 12, 72074 Tübingen, Germany
e-mail: dominik.hoeyng@uni-tuebingen.de

F. M. D'Affonseca
TIMGEO GmbH, Hölderlinstr. 29, 72074 Tübingen, Germany

P. Bayer
Geological Institute, ETH Zurich, Sonneggstr. 5, 8092 Zurich, Switzerland

E. G. de Oliveira · J. A. J. Perinotto · F. Reis
Instituto de Geociências e Ciências Exatas, UNESP, Univ. Estadual Paulista, Av. 24-A n° 1515 – B. Bela Vista, 13506-900 Rio Claro, SP, Brazil

H. Weiß
Helmholtz Center for Environmental Research (UFZ), Permoserstr. 15, 04318 Leipzig, Germany

Introduction

Progressive increase in groundwater resource development and depletion, along with strong urban development, has been placing stress on the transboundary Guarani aquifer system (GAS), which underlies the countries of Brazil, Argentina, Paraguay and Uruguay in South America (Fig. 1). The GAS is mostly confined and direct recharge occurs only in its outcropping areas, which add up to 10 % of the total GAS area (Rabelo and Wendland 2009). Brazil alone accounts for more than 90 % of the withdrawal from a total volume of 1,039 M m^3 per year, where 80 % of this volume is abstracted in São Paulo State (Schmidt and Vassolo 2011). The release of agro-chemicals caused by intense agro-industrial activities (e.g. sugar cane production in São Paulo State) in the GAS recharge areas, mean a high pollution threat. Moreover, accidental or uncontrolled discharge of domestic wastes or manufactured persistent chemicals in the GAS recharge areas (e.g. Lago et al. 2009) pose a high risk for long-term groundwater contaminations,

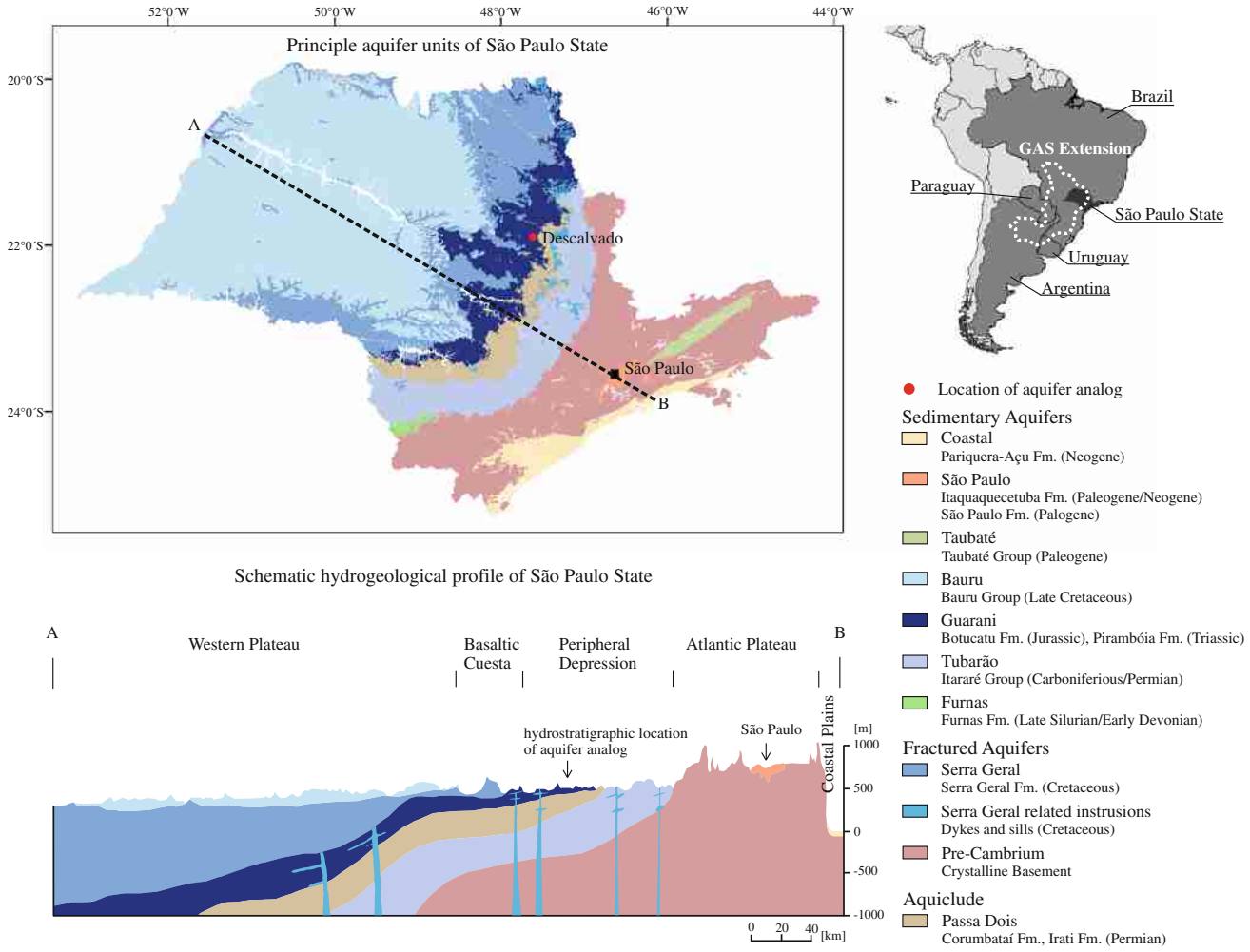

Fig. 1 GAS extension [after Araújo et al. (1999)] and schematic hydrostratigraphic map and profile of São Paulo State (modified after: DAEE; IG, IPT; CPRM. *Mapa de Águas Subterrâneas do Estado de São Paulo*. São Paulo 2005) and the location of the aquifer analog

adding further strain on this relevant groundwater reservoir (Goldemberg et al. 2008; Dantas et al. 2011; Marimon et al. 2013).

Although a deep understanding of surface/subsurface and surface/atmosphere interactions is crucial for a sustainable water quality management on a catchment and basin scale (Grathwohl et al. 2013), a comprehensive and detailed knowledge of the spatial distribution of hydraulic parameters on a local scale is necessary for proper planning of any groundwater protection and remediation action (Comunian et al. 2011). Realistic representation of these parameters in mathematical models is challenging and needed for reliable prediction of groundwater flow and contaminant transport (Whittaker and Teutsch 1999). However, as economic and practical constraints often restrict proper aquifer characterization, crucial hydrogeological features may remain unnoticed (e.g. Parker et al. 2008), resulting in high degrees of uncertainty and, consequently, in model impreciseness.

The use of reservoir analog models is an established alternative approach to support and improve the characterization and conceptualization of groundwater (e.g. Whittaker and Teutsch 1999; Klingbeil et al. 1999; Huggenberger and Aigner 1999; Heinz et al. 2003; Bersezio 2007; Bayer et al. 2011) and hydrocarbon reservoirs (e.g. Flint and Bryant 1993; Pringle et al. 2006). Information on the spatial variability of groundwater reservoir parameters for the construction of aquifer analogs can either be generated by structure-imitating, process-imitating or by descriptive approaches (Koltermann and Gorelick 1996). Numerous aquifer analog studies reproduce the sedimentary structures and the corresponding hydraulic properties of different depositional environments (e.g. Sweet et al. 1996; Bersezio et al. 1999; Weissmann et al. 1999; Anderson et al. 1999; Hornung and Aigner 1999; Heinz et al. 2003; Cardenas and Zlotnik 2003; Heinz and Aigner 2003; Bersezio et al. 2004, 2007; Kostic et al. 2005; Felletti et al. 2006; Zappa et al. 2006; Kessler et al. 2012). For instance, Bayer et al. (2011)

successfully constructed a high-resolution aquifer analog of high-energy environment deposits (e.g. braided river channels), where hydraulic properties significantly vary on a centimeter to decimeter scale, vertically and horizontally.

The enormous capacity and economic significance of the GAS have made this groundwater reservoir subject to multinational and multi-disciplinary research efforts to use this resource in a sustainable manner for current and future demand (e.g. Puri et al. 2001). Although comprehensive studies have been conducted to characterize and understand the hydrogeology and hydrogeochemistry of this system (e.g. Wendland et al. 2007; Soares et al. 2008; Foster et al. 2009; Zuquette et al. 2009; Hirata et al. 2011; Gastmans et al. 2012; Bonotto 2012, 2013), no high-resolution description of its hydrogeological and sedimentological facies exist.

According to Donatti et al. (2001), in São Paulo State the GAS consists of a Triassic succession of siltstones, sandy siltstones, sandstones and coarse to pebbly sandstones of a wet-aeolian system (Pirambóia Formation), followed by Jurassic dune deposits of a dry-aeolian system (Botucatu Formation,). The wet-aeolian system is characterized by a higher phreatic level due to the vicinity to the coast (Donatti et al. 2001). Coarser sediment was supplied by discharging streams and rivers, cutting into the aeolian deposits and resulted in a fluvial–aeolian facies association. In contrast to the homogeneous aeolian deposits of the Botucatu Formation, the heterogeneous fluvial–aeolian sediments, where channel deposits intermingle with well-sorted aeolian sands are of particular relevance in the upper part of the Pirambóia Formation. Groundwater flow patterns are potentially non-uniform and complex in those aquifer portions and therefore, a general understanding of the heterogeneous architecture is required to assist the prediction of plume geometry and evolution in case of a possible contamination on a local scale. Extensive sedimentological investigations of this sedimentary unit has already been carried out (Caetano-Chang and Wu 2006; Dias and Scherer 2008), nevertheless no previous study investigated the heterogeneity and hydrogeological role of these fluvial–aeolian deposits within the Pirambóia Formation, as well as in the overall context of the GAS in São Paulo State.

This work is the first application of the aquifer analog approach at the GAS for fluvial–aeolian sediments deposited in a transitional environment of a wet-aeolian system. In order to understand the specific hydraulic characteristics of the fluvial–aeolian sediments occurring at the upper part of the Pirambóia Formation, an aquifer analog is constructed from sedimentary outcrops in a sandy open-pit mine. For that purpose, three parallel and equally spaced vertical outcrops were investigated according to the common aquifer analog construction procedure (e.g. Anderson et al. 1999; Bersezio et al. 1999; Heinz and Aigner 2003; Bayer et al. 2011). Additionally, two perpendicular outcrops were recorded during pit excavation. It facilitates the reconstruction of the sediment body geometries between two parallel main sections and enables the assemblage of a quasi-three-dimensional (3D) model (e.g. Felletti et al. 2006; Kessler et al. 2012). It also minimizes, for instance, the uncertainties inherent to geostatistical models of aquifer analogs without perpendicular sections, such as the one developed by Comunian et al. (2011). In order to capture the fine-scale heterogeneity of the fluvial–aeolian facies association, sedimentary facies were mapped on a centimeter scale. Hydrogeological investigations were conducted in the field and laboratory. The combined geological analysis of sedimentary structures and determination of hydraulic properties (K, n) enables, for the first time, the identification of the most important elements of heterogeneity in terms of preferential flow paths, connectivity, and high permeable facies of the fluvial–aeolian deposits of the Pirambóia Formation on a local scale. Hydrofacies types are derived and the 2D spatial K distribution of the examined sediments is related to the lithofacies and represented a quasi-three-dimensional aquifer analog model consisting of 2D cross-sectional profiles.

Guarani aquifer system

Sedimentology

The GAS belongs to the most important groundwater reservoirs in the world and is the biggest groundwater system in South America. With a storage volume of some 40,000 km^3, it underlies a total area of about 1,200,000 km^2 in Brazil, Paraguay (both Paraná Basin), Argentina (Chaco-Paraná Basin), and Uruguay (North Basin) (Puri et al. 2001). The accumulated thickness of the sedimentary and igneous rocks filling up the Paraná and Chaco-Paraná basins is about 8,000 m. The Paraná basin comprises six super-sequences bounded by unconformities from the Lower Ordovician (450 M years) to the Upper Cretaceous (65 M years), which represent major transgressive–regressive cycles and continental sedimentation and erosion processes (Milani et al. 1998).

The groundwater-hosting formations comprising the GAS are built up of weakly-cemented, mainly continental siliciclastic sedimentary rocks of Triassic and Jurassic age (~250–145 M years) (Fig. 1), deposited on a Permo-Triassic erosional surface (250 M years) (Assine et al. 2004) during progressive continentalization of Western Gondwana at a late stage of the complex geologic evolution of the Paraná basin (Hirata et al. 2011). The end of the basin evolution is marked by Early Cretaceous thick basalt layers (~1,500 m) of the Serra Geral Formation, which extensively cover and confine the GAS. The average thickness of the GAS sediments is about 250 m, but it greatly varies from more than 600 m to less than 50 m (Foster et al. 2009). Almost

two-thirds of the transboundary aquifer system in the Paraná basin are located on Brazilian territory.

In São Paulo State (Brazil), the GAS is formed by siltstones, sandy siltstones, sandstones and coarse to pebbly sandstones of the Pirambóia Formation and aeolian sandstones of the Botucatu Formation (Fig. 1). For São Paulo State, an overall thickness for the Pirambóia Formation of 75–270 m and of 20–238 m for the Botucatu Formation is reported (Hirata et al. 2011). The lower and upper boundaries of the GAS are defined by the occurrence of coastal siltstones (e.g. Corumbataí Formation) and basalt layers (Serra Geral Formation), respectively (Donatti et al. 2001). Although the Pirambóia and the Botucatu Formation are often regarded as a single unit from a groundwater reservoir perspective, they differ in terms of age, deposition and diagenetic evolution (Hirata et al. 2011). Several studies address facies characteristics, rock properties, and distinct depositional environment for the Pirambóia (wet-aeolian system) and Botucatu Formation (dry-aeolian system), and correlate them to present environments for an in-depth understanding of the depositional system (e.g. Donatti et al. 2001; Assine et al. 2004). According to Donatti et al. (2001), the sandstone succession comprising the GAS in São Paulo State can be subdivided into five main facies associations: (1) tidal plain with aeolian sand sheets; (2) coastal dunes with frequently flooded interdune flats; (3) coastal dunes with rarely flooded interdune flats; (4) braided alluvial plain with aeolian dunes; (5) giant dunes with interdune depressions. Facies associations 1–4 correspond to the Pirambóia Formation, while facies association 5 is related to the Botucatu Formation.

The fluvial–aeolian sandstones of the upper part of the Pirambóia Formation (facies association 4), the focus of this study, crop out in the central-eastern part of São Paulo State in the vicinity of the cities of Descalvado, Itirapina and São Pedro with a varying thickness from a few meters up to approximately 45 m (Caetano-Chang and Wu 2006). This facies association shows fluvial deposits of braided rivers reworked by the prevailing winds and mixed with aeolian dune deposits (Caetano-Chang and Wu 2006).

The coarse-grained sandstones and conglomerates of the top of the Pirambóia Formation are mainly quartzarenites (mineralogically supermature) and rarely subarcosean (considered to be mature to submature). The cement occurring at the upper Pirambóia Formation consists of iron oxide and autogenic clay, adhering to the surface of the grains or partially filling the pores. Calcite and, to a lesser extent, locally pyrite might occur as patches that cement grains (Caetano-Chang and Wu 2006). In the contact zone with the mafic dykes and sills of the Serra Geral Formation (Fig. 1), the deposits of the Pirambóia Formation can be locally "cooked" due to contact metamorphism.

Area of investigation

The study area is located in the recharge area of the GAS at the central-eastern part of São Paulo State (Brazil), in the vicinity of Descalvado city (Fig. 1). Here, the basalts of the Serra Geral Formation and the sandstones of the Botucatu Formation are eroded, and the sandstones of the Pirambóia Formation crop out and appear as bedrock, partially superimposed by Tertiary sandy deposits of the Santa Rita do Passa Quatro Formation. Here, the Pirambóia Formation is slightly weathered and the deposits partially cemented with iron oxide and autogenic clay. There are no digenetic overprints in the area of investigation from Serra Geral-related intrusions. The field site is situated in a sandy open-pit mine with multiple levels of operation in the Pirambóia Formation, where sand is excavated from contiguous banks.

Several locations in the open-pit mine were inspected and compared in terms of the appearance of typical and common sedimentary features of the fluvial–aeolian deposits of the upper part of the Pirambóia Formation. Based on characteristic structures of the fluvial–aeolian sediments and on operational feasibility issues, a suitable outcrop was selected in the central part of the open-pit mine for the aquifer analog construction. The geographical coordinates of the outcrop are: 21°56′46.5″S, 47°36′45.8″W. The selected sand bank provided ideal insights into the physical heterogeneities and allowed a centimeter-scale depiction of the existing lithofacies and hydrofacies.

Methods of work

Fieldwork and mapping procedure

The overall dimension of the selected, rectangular-shaped sand body is 28 m in length (Lx), 7 m in width (Ly), and 5.8 m in height (Lz). A set of poles and markers were equidistantly placed along each outcrop face as reference points for the mapping procedure and photographic documentation. In order to characterize the spatial variations of sedimentary structures in three dimensions, three parallel cross-sections (spacing 3.5 m along the y-axis) and two perpendicular lateral sections at $x = 0$ m and $x = 28$ m were constructed by stepwise horizontal excavation of the selected sand bank, as schematically illustrated in Fig. 2. First, the original outcrop wall (section A–A′) was mapped (Fig. 2a) and afterwards, the sand body carefully excavated by 3.5 m. Subsequently, the exposed new frontal outcrop wall (section B–B′) and the first part of the lateral outcrop walls (A–C, A′–C′) were recorded (Fig. 2b). Again, the sand body was excavated by 3.5 m to map the section C–C′ and the second part of the lateral outcrop walls (A–C, A′–C′) (Fig. 2c).

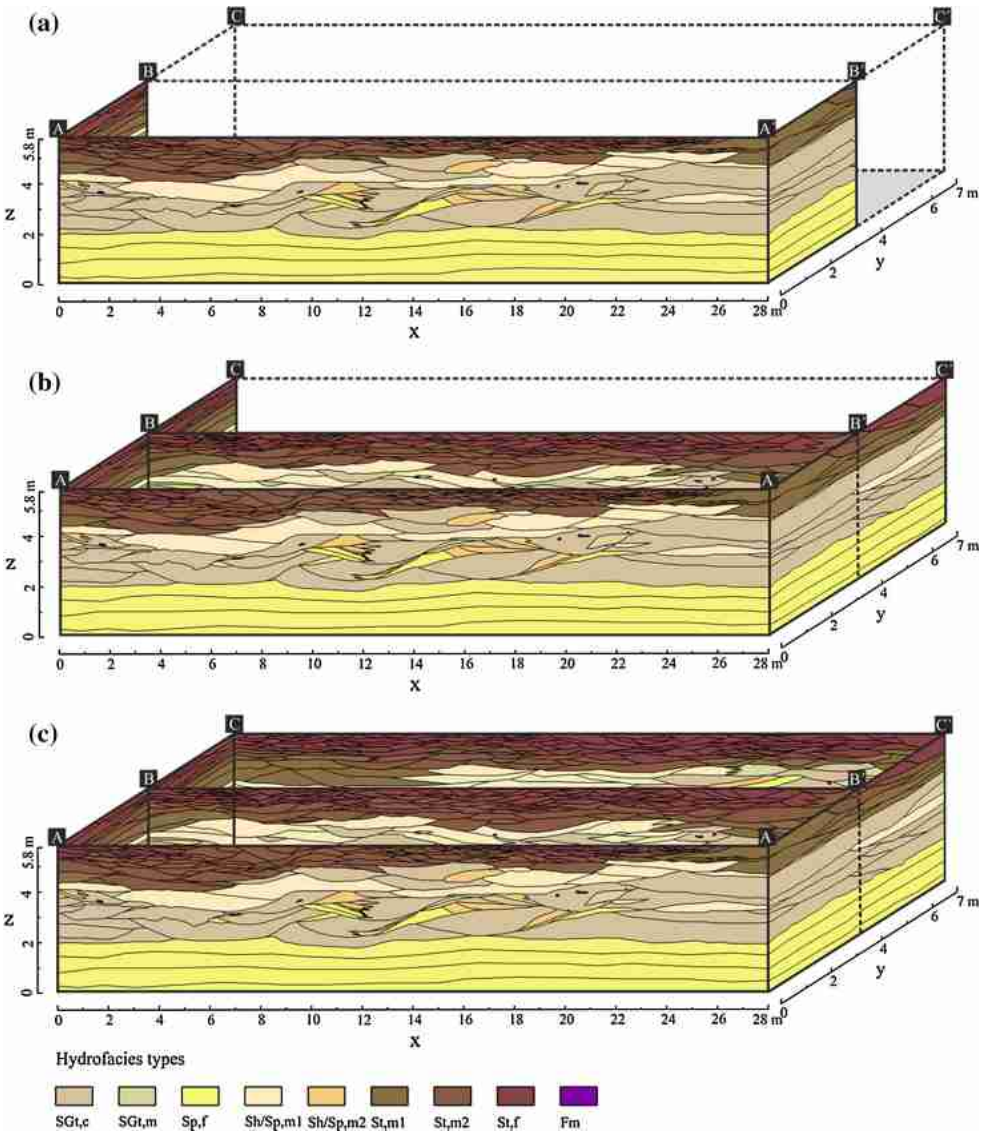

Fig. 2 Schematic representation of the stepwise quasi-three-dimensional aquifer analog model construction process and the geometry and distribution of the identified hydrofacies at **a** section A–A′ and first half of the lateral sections A–C and A′–C′, **b** section B–B′ and second half of the lateral sections A–C and A′–C′, **c** and section C–C′. For illustrative purposes, the longitudinal extension of the lateral sections is exaggerated by a factor of 1.2

The mapping process was assisted by systematic description and sedimentological interpretation of the complex structured sediments. The sedimentary structures were recorded in the field with a 5 cm × 5 cm resolution, producing outcrop maps at a 1:50 scale for posterior data processing. Close-up photographs of the entire outcrop were taken to provide basic digital images.

Lithofacies types were depicted following the approach proposed by Miall (1978). This method is based on a two-letter scheme, allowing the categorization of sedimentary units on the basis of their sedimentary structures and genetic processes. The dominant grain size is indicated by a capital letter (G = gravel, S = sand, F = fine-grained facies, including silt and mud), whereas the lowercase letters describe the characteristic texture and structure of the lithofacies (t = trough bedded, h = horizontal, p = planar, m = massive). In case of equal shares of two dominant grain sizes, a combination of both is employed.

A comprehensive sediment sampling campaign from multiple locations over each outcrop was carried out in order to allow the determination of the hydraulic properties of each lithofacies types in the laboratory by means of grain size analysis. In order to validate the laboratory-derived hydraulic conductivity estimates by infiltration test, wells were temporarily installed on top of the outcrop bench and in front of the outcrop prior to excavation. Due to restrictions during the ongoing mining operations, only five wells (depth: 0.5 m) could be installed. The infiltration tests were performed for three hydraulic conductivity zones using a constant-head (Guelph permeameter) and a falling-head well permeameter. The wells with a depth of 0.5 m were located at $x = 7$ m, $y = 1.5$ m, and from $z = 5.3$ m to 5.8 m, at $x = 27$ m, $y = 1.5$ m, and from $z = 5.3$ m to 5.8 m, and right in front of the first outcrop at $x = 23$ m, $y = 0$, and from $z = 0$ m to -0.5 m.

Laboratory work

Empirical grain-size methods for the estimation of hydraulic conductivity, *K*, in porous media are standard in hydrogeological practice (Vukovic and Soro 1992; Kasenow 2002; Carrier 2003). For the collected samples, grain size analysis was carried out by sieving (Tyler sieves with a mesh size from 0.053 to 31.7 mm for the gravel and sand fraction). A laser diffraction method served for characterization of the fines distribution (<0.053 mm, Malvern Mastersizer 2000, Malvern Instruments). The total porosity, *n*, was determined by direct methods in the laboratory from undisturbed field samples for all hydrofacies types (total number of samples = 62) (Table 1).

Since the Kozeny–Carman formula and the US Bureau of Reclamation (USBR) formula are not applicable for the estimation of hydraulic conductivity in silt and clay materials, a falling-head permeameter test was alternatively conducted in the lab on irregular shaped, undisturbed clay samples of only a few decimeters in size. However, because the classical falling-head method requires a regular, geometric shape of the sample (ABGE 1981), an approach for irregular-shaped, undisturbed bulk samples developed by Oliveira (2000) was employed instead.

Aquifer analog model construction

Determination of hydraulic properties and hydrofacies types

The lithological classification only considers the main grain size classes as previously described (e.g. G = gravel, S = sand, F = fines) and does not embrace the varying proportions of the subclasses of the grain size spectrum (e.g. fine sand, medium sand, coarse sand), which may significantly influence the hydraulic properties within a single lithofacies. Different lithofacies may have variable hydraulic properties and therefore, from a hydrogeological perspective, a translation into hydrofacies types is required to describe the permeability distribution and hydraulic connectivity within the aquifer. The term 'hydrofacies' is defined as a relatively homogeneous but anisotropic and hydrogeologically meaningful unit (Anderson 1989; Poeter and Gaylord 1990), which has a horizontal-correlation length that is finite, but that in most cases, is significantly greater than the vertical correlation length (Anderson 1989). The determination of hydrofacies types, therefore, allows for recognizing preferential flow paths, low permeable flow units and flow barriers, and helps to quantitatively describe the flow parameter distribution of the reservoir (Klingbeil et al. 1999; Heinz et al. 2003), which is the ultimate objective of the aquifer analog construction.

For that reason the different hydraulic conductivities of each lithofacies are determined by the widely accepted Kozeny–Carman formula and the USBR formula (Vukovic and Soro 1992; Kasenow 2002). For the latter, the value for kinematic viscosity of water is related to a temperature of 20 °C. To reflect the grain size spectra for different hydrofacies types and corresponding *K* values, a classification scheme according to DIN EN ISO 14688-1 (2002) is applied. This scheme uses capital letters for the dominant, grain size class of the hydrofacies type (e.g. CSa = coarse sand, MSa = medium sand, FSa = fine sand). Minor grain size mass fractions are indicated by small letters in

Table 1 Lithofacies and hydrofacies types with hydraulic properties

Lithofacies (after Miall 1978)	Hydrofacies code used	Hydraulic conductivity *K* (m/s)	Porosity *n* (-)	Number of samples	Hydrofacies classified after DIN EN ISO 14688-1 (2002)
SGt	SGt,c	$2.96 \times 10^{-4} \pm 9.90 \times 10^{-5}$[a]	0.32 ± 0.04	7	Sa/Gr
	SGt,m	$9.44 \times 10^{-5} \pm 6.60 \times 10^{-5}$[a]	0.32 ± 0.04	7	fgr′fsamsaCSa
Sp	Sp,f	$1.63 \times 10^{-4} \pm 1.74 \times 10^{-5}$[b]	0.25 ± 0.05	9	msaFSa
Sh/Sp	Sh/Sp,m1	$1.38 \times 10^{-3} \pm 6.88 \times 10^{-5}$[b]	0.33 ± 0.05	8	fsa′csaMSa
	Sh/Sp,m2	$7.77 \times 10^{-5} \pm 3.05 \times 10^{-5}$[a]	0.33 ± 0.05	6	csa′fsa*MSa
St	St,m1	$5.97 \times 10^{-5} \pm 2.91 \times 10^{-5}$[a]	0.29 ± 0.04	7	csa′fsaMSa
	St,m2	$2.49 \times 10^{-5} \pm 1.34 \times 10^{-5}$[a]	0.29 ± 0.04	6	si′csa′fsa*MSa
	St,f	$6.23 \times 10^{-6} \pm 5.25 \times 10^{-6}$[a]	0.24 ± 0.05	7	si′msa*FSa
Fm	Fm	$7.84 \times 10^{-8} \pm 4.22 \times 10^{-8}$[c]	0.29 ± 0.03	5	Cl

Hydrofacies code: *SGt,c* trough cross-bedded coarse sand and gravel, *SGt,m* trough cross-bedded medium sand and gravel, *Sp,f* planar cross-bedded fine sand, *Sh/Sp,m1* horizontally laminated to planar cross-stratified medium sand, *Sh/Sp,m2* horizontally laminated to planar cross-stratified medium sand with fine sand, *St,m1* trough cross-bedded medium sand, *St,m2* trough cross-bedded medium sand with find sand, *St,f* trough cross-bedded fine sand, *Fm* massive clay intraclasts

[a] Derived by empirical equation according to Kozeny–Carman

[b] Derived by empirical equation according to USBR

[c] From laboratory permeameter tests

ascending order in front of the main classes, which can be further denoted with an apostrophe in case they are minor or with an asterisk if they are prominent (e.g. csa′fsa*M-Sa = medium sand with a very minor portion of coarse sand and a prominent portion of fine sand).

Although this scheme is a precise way to reflect grain size shares in a letter-based code, it is rather elusive for fast comprehension. Therefore, a convenient and more intuitive hydrofacies code based on the lithofacies code is applied in this study. The employed code uses similar letters as the lithofacies code, indicating sedimentary structures, a small letter to denote the dominant grain size (f = fine, m = medium, c = coarse) and a number for further differentiation if necessary. The lithofacies and hydrofacies recorded and classified in this study, as well as the hydraulic properties, are summarized in Table 1.

Model construction

The outcrop-based sedimentological and the hydrogeological information was stored in a database and subsequently linked to digital high-resolution images. One individual panorama image was created for each outcrop. The panorama images were produced by assembling multiple high-resolution and overlapping close-up terrestrial outcrop orthophotos. To avoid optical distortion effects from the left and right side of the photograph, a share of 25 % was cut following the approach of Morales et al. (1997). Subsequently, the remaining center parts of the photographs were stitched together using Corel DRAW X5. The obtained 2D photo-panels were then used for onscreen digitization with a GIS software (ArcGIS 9, ESRI®), encompassing the following steps: (1) sedimentary structures and forms were delineated as polygons based on the outcrop images and generated field maps; (2) each constructed polygon constituting a single hydrofacies was attributed to the respective hydrofacies code and hydraulic parameters from the sedimentological and hydrogeological database; (3) the digitized hydrofacies assemblages from outcrop data were saved as shapefiles and converted into grid format with specified cell size and number in order to use the aquifer analog for future numerical modeling experiments.

Results and discussion

In the examined upper part of the Pirambóia Formation, conglomeratic pebbly and coarse sands interspersed with very poorly sorted fine-to-coarse pebbles were found adjacent to clean and very well-sorted and well-rounded, medium-to-fine sand with minor amounts of fines. The sands often gradually intermingle with pebbly and coarse deposits, locally containing large pieces of clay (up to 50 cm in diameter).

Based on the outcrop analysis, five distinctive lithofacies are recognized on the basis of their primary sedimentary features. The five lithofacies and their corresponding hydraulic properties are described in detail hereafter and summarized in Table 1. The order of the description is based on the main occurrence of the facies from the bottom to the top of the outcrops.

Planar cross-bedded aeolian sand lithofacies (*Sp*)

Geological description

This lithofacies appears in the outcrops mainly at $z \leq 2$ m, with some localized occurrence at 3 m $\leq z \leq 4$ m, composing approximately 35 % of the outcrop area based on the three main cross-sections. The most prominent feature of the *Sp* lithofacies is the clean and very well-sorted and well-rounded, medium-to-fine sands with minor amounts of silt deposited under aeolian conditions (Fig. 3d). The primary sedimentary structure is characterized by low dipping foresets ($\sim 15°$) of planar cross-beds and horizontal to subhorizontal lamina. The sets of cross-strata have an average thickness of ~ 50 cm. Drill cores executed in front of the outcrop confirmed a minimum thickness of ~ 2.5 m of this sand package. The upper part of the cross-stratified foresets has been eroded and covered by coarse fluvial deposits (*SGt* lithofacies), indicating an erosional surface (Fig. 3d).

Hydraulic characterization

For the homogeneous aeolian sands of the *Sp* lithofacies a hydraulic conductivity value of $1.63 \times 10^{-4} \pm 1.74 \times 10^{-5}$ m/s ($n = 0.25 \pm 0.05$) is obtained, defining the hydrofacies type *Sp,f* (hydrofacies type *Sp,f* = planar cross-bedded fine sand) (Fig. 4a–d). The hydraulic conductivity of the field test performed at the location $x = 23$ m, $y = 0$, and from $z = 0$ m to -0.5 m, which refers to this hydrofacies, is $K = 6.6 \times 10^{-4}$ m/s. Although the field derived value is in agreement with the laboratory determined values, it has to be treated with caution. The field test was carried out with great care but possible effects of the mining operations, such as soil compaction or occurrence of small fissures, might adversely influence data reliability. Thus, the field values only serve well for a rough cross-check of laboratory-derived values.

Trough cross-bedded sand and gravel lithofacies (*SGt*)

Geological description

This is the main lithofacies occurring from 2 m $\leq z \leq 5$ m in the outcrops, representing a total area fraction of ~ 30 % of the three main cross-sections, with restricted occurrence

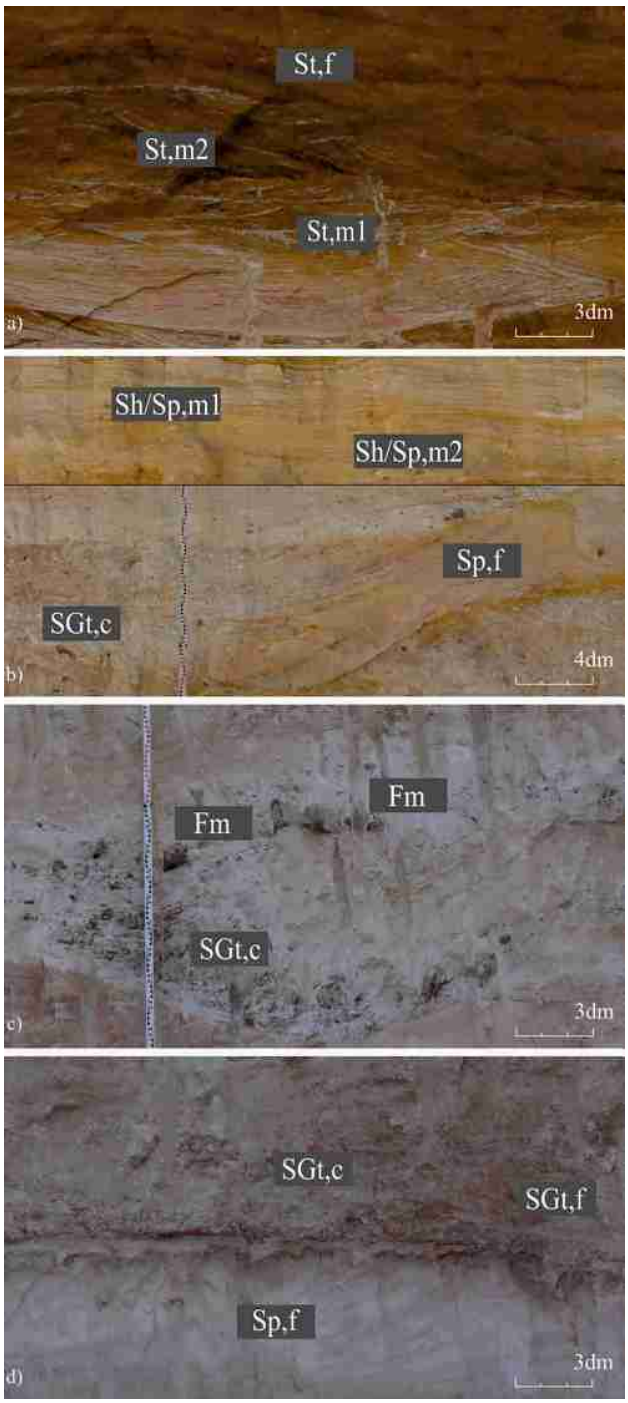

Fig. 3 Photographs of identified lithofacies and corresponding hydrofacies types in the outcrop: **a** trough cross-bedded sand lithofacies (*St*), **b** horizontally laminated to planar cross-stratified sand lithofacies (*Sh/Sp*), **c** trough cross-bedded sand and gravel lithofacies (*SGt*) with massive clay intraclasts (*Fm*), **d** planar cross-bedded aeolian sand lithofacies (*Sp*) and overlying lithofacies (*SGt*)

around $z = 5.5$ m. The *SGt* lithofacies are built up of a mixture of chaotically structured conglomeratic pebbly and coarse sands, with varying amounts interspersed with very poorly sorted fine-to-coarse pebbles. The deposits are presented as bodies of channel-shape geometry (Fig. 3c), varying vertically and horizontally in size between ~0.5 and 3 m and ~0.3 and 1.5 m, respectively. The pebbles are angular to rounded and mixed with coarse sand and clay fragments in a silt matrix. Large irregularly shaped intraclasts of dark reddish clay (lithofacies *Fm*) of a few decimeters in size can be found in these deposits (Fig. 3c). The sediment bodies often internally cut into each other, both laterally and vertically. Along the margin of the channel bodies, the deposits frequently interfinger and interbed with medium and fine-grained, well-sorted sands of the *Sh/Sp* lithofacies (Fig. 3b), which are described later in detail. The strata of the *SGt* lithofacies display an irregular, lower bounding surface sitting on top of the aeolian well-sorted fine sands (*Sp* lithofacies) (Fig. 3d). The medium-scale channel fills observed in the outcrop reveal a typical trough cross-bedded structure. They can be interpreted on the basis of their multiple erosional surfaces and coarse-grained and pebbly nature as the depositional response to high-energy fluvial processes of a braided river channel system bearing a heavy suspended bed load.

Hydraulic characterization

Varying amounts of pebbles and coarse sand of the *SGt* lithofacies result in two different hydrofacies (hydrofacies type *SGt,c* = trough cross-bedded coarse sand and gravel; and *SGt,m* = trough cross-bedded medium sand and gravel). The *SGt,c* hydrofacies vary by equal amounts of sand and gravel over all grain size classes (very fine to coarse) with an estimated mean hydraulic conductivity of $K = 2.96 \times 10^{-4} \pm 9.90 \times 10^{-5}$ m/s and $n = 0.32 \pm 0.04$. The *SGt,c* hydrofacies dominate the *SGt* lithofacies. In the areas where the *SGt* lithofacies predominantly consist of coarse sand with portions of medium and fine sand, the hydrofacies type *SGt,m* is defined, with a $K = 9.44 \times 10^{-5} \pm 6.60 \times 10^{-5}$ m/s and $n = 0.32 \pm 0.04$. Overall, this lithofacies contains a significant amount of fines. The higher surface area of small size grains increases the frictional resistance of flow and reduces the intrinsic permeability of sediments (Fetter 2001), which is reflected by a rather low *K* value for this coarse, pebbly sand.

Massive clay intraclasts (*Fm*)

Geological description

At some positions in the outcrop (e.g. Fig. 2a, at location: $x = 20.8$ m, $z = 4$ m), randomly oriented, dark brownish, irregularly shaped intraclasts of clay can be found embedded in the coarse fluvial deposits of the *SGt* lithofacies (Fig. 3d). The size of the muddy intraclasts ranges from a few centimeters up to several decimeters. The

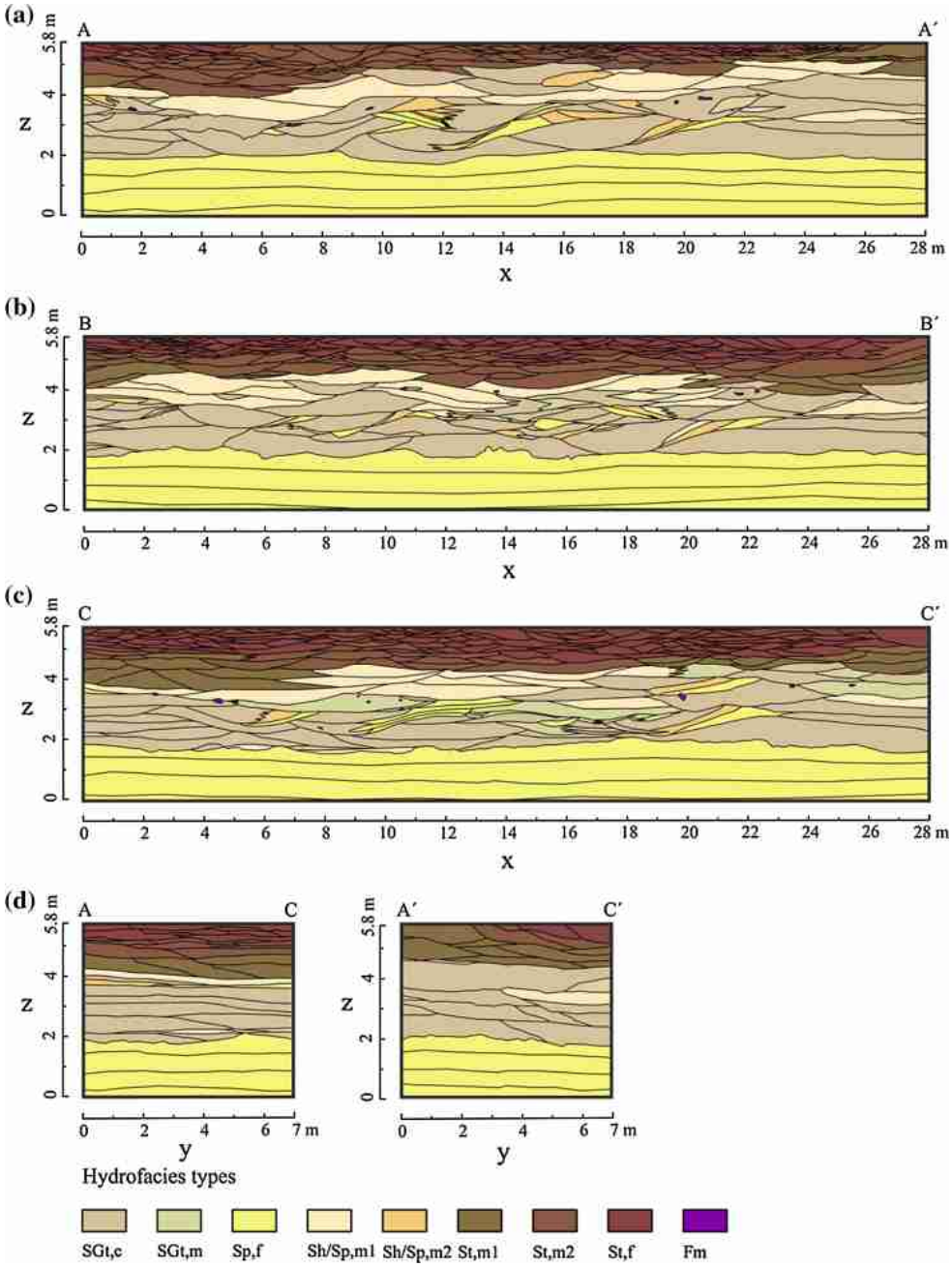

Fig. 4 Geometry and distribution of the identified hydrofacies at the aquifer analog frontal sections **a** A–A′, **b** B–B′, **c** C–C′, and lateral sections **d** A–C and **e** A′–C′

intraclasts can be attributed to reworked, thin muddy layers of floodplains from marginal channels in a braided river environment or from small and ephemeral lakes.

Hydraulic characterization

The obtained hydraulic conductivity for the hydrofacies type *Fm* (hydrofacies type *Fm* = massive clay intraclasts) is very low ($K = 7.84 \times 10^{-8} \pm 4.22 \times 10^{-8}$ m/s, $n = 0.29 \pm 0.03$). However, these hydrofacies are discontinuous and of minor presence in the outcrops (total area fraction of <1 % within the three main cross-sections). Therefore, from a hydrogeological point of view it is not considered relevant in the examined aquifer analog.

Horizontally laminated to planar cross-stratified sand lithofacies (*Sh/Sp*)

Geological description

This lithofacies locally appears from 2 m $\leq z \leq$ 5 m (total area fraction of $\sim$11 % within the three main cross-sections) within the *SGt* lithofacies. It is characterized by laminated sheets, small bodies and lenticular units of very

well-sorted medium to very fine sands (Fig. 3b). The small bodies and lenticular units of sand either occur as wedges along the margins of coarse grained channel fills exhibiting internal cross-stratification (*Sp*), or as relatively laterally continuous laminated sheets (*Sh*). The medium to very fine sands along the sides of the channel display a prominent complex interfingering pattern and gradual changes with the pebbly sands of the *SGt* lithofacies (Fig. 3b).

This junction of coarse fluvial deposits with fine aeolian sands is a common sedimentological feature for wet-aeolian systems, where during the wet period fluvial processes prevail, and in the dry season wind reworks fluvial deposits and supplies fine sand into the system (Assine et al. 2004; Caetano-Chang and Wu 2006). The eroded wedges and lenticular units of fine sand present vestiges of the aeolian influence on the depositional system. Plane sandy bed forms are associated with fluvial processes and can be rather attributed to upper flow regime conditions, as lower flow regime conditions are characterized by cross-stratified sands under a waning current velocity (Miall 2010).

Although the deposits of the study site are carefully mapped, how the sedimentary bed forms evolve between two parallel outcrops could not always be clearly derived. Gradual changes of the internal stratification from horizontal to cross-stratified are frequently observed. Therefore, for practical reasons, the lithofacies classes *Sh* and *Sp* are merged (*Sh/Sp*) and treated as one facies class for the outcrop.

Hydraulic characterization

The grain size ranges mainly from fine to medium sand, but also includes varying amounts of fine and coarse sand. This allows a classification of the *Sh/Sp* lithofacies into three different hydraulically relevant units (hydrofacies type *Sh/Sp,m1* = horizontally laminated to planar cross-stratified medium sand; *Sh/Sp,m2* = horizontally laminated to planar cross-stratified medium sand with fine sand; *Sp,f* = planar cross-bedded fine sand). The *Sh/Sp,m1* hydrofacies type shows the highest hydraulic conductivity observed in the outcrops, with $K = 1.38 \times 10^{-3} \pm 6.88 \times 10^{-5}$ m/s ($n = 0.33 \pm 0.05$). The fine parts of the lithofacies class *Sh/Sp* have the same hydraulic properties as the previously described aeolian lithofacies (*Sp*). Thus, the fine parts of the lithofacies *Sh/Sp* can also be denoted as hydrofacies type *Sp,f* with $K = 1.63 \times 10^{-4} \pm 1.74 \times 10^{-5}$ m/s and $n = 0.25 \pm 0.05$.

Trough cross-bedded sand lithofacies (*St*)

Geological description

The *St* lithofacies are observed in the outcrops at 4.5 m $\leq z \leq$ 5.8 m (total area fraction of 24 % within the three main cross-sections) and primarily consist of sets of trough cross-bedded very fine to medium sand (Fig. 3a). The trough beds are commonly at the decimeter to meter scale and are formed by well to poorly sorted, rounded grains. This lithofacies can be separated into three different sets based on the grain size and the degree of coating with detrital ferric hydroxides of syndepositional origin. The trough beds of moderately sorted white medium sand with portions of fine and coarse sands are followed by trough beds of light brownish color including higher portions of fines. On top, sets of very well sorted, very fine to fine sand of dark brown color are identified. The trough bed forms can be interpreted as subaqueous sinuous-crested 3D dunes. The term 'dunes' can be synonymously used for sand bars in river channels to interpret trough cross-bed stratification.

Hydraulic characterization

Following the grain size distribution of the trough beds, three different hydrofacies can be distinguished for the *St* lithofacies (Table 1). The dark brown sets of fine sand (hydrofacies type *St,f* = trough cross-bedded fine sand) show a low hydraulic conductivity of $K = 6.23 \times 10^{-6} \pm 5.25 \times 10^{-6}$ m/s ($n = 0.24 \pm 0.05$). The coarser sets have hydraulic conductivities of $K = 5.97 \times 10^{-5} \pm 2.91 \times 10^{-5}$ m/s (hydrofacies type *St,m1* = trough cross-bedded medium sand) and $K = 2.49 \times 10^{-5} \pm 1.34 \times 10^{-5}$ m/s (hydrofacies type *St,m2* = trough cross-bedded medium sand with find sand) ($n = 0.29 \pm 0.04$ for both types). Field tests were performed on top of the outcrop at the locations $x = 7$ m, $y = 1.5$ m and $z = 5.8$ m to 5.3 m for the hydrofacies type *St,m2* and at $x = 27$ m, $y = 1.5$ m and $z = 5.8$ m to 5.3 m for the hydrofacies type *St,m1*. The received data from the Guelph permeameter test (*St,m1*: $K = 6.85 \times 10^{-5}$; *St,m2:* $K = 6.80 \times 10^{-5}$ m/s) and falling-head permeameter test (*St,m1*: $K = 1.78 \times 10^{-5}$; *St,m2* $K = 2.17 \times 10^{-5}$ m/s) are in the same range as the laboratory values. Although field derived values approximate the laboratory data well, the data are only suitable for a rough cross-check due to low data quantity and afore mentioned situation in the outcrop.

Hydrogeology of entire aquifer analog

The spatial distribution of the previously described lithofacies and hydrofacies reveals a distinctive succession throughout all outcrop sections. As shown in Fig. 4, three genetic units can be determined from the bottom to the top of the outcrop: (1) a continuous layer of aeolian sands (*Sp,f* hydrofacies) at $z < 2$ m (2) braided river channel deposits of pebbly to fine sands of the hydrofacies types *SGt,c*; *SGt,m* with clay intraclasts (*Fm*), plane sandy bed forms and cross-bedded medium sands of the hydrofacies types *Sp,f*; *Sh/Sp,m1*and *Sh/Sp,m2* at 2 m $\leq z \leq$ 4 m; (3)

fluvial sets of cross-bedded medium to fine sands of the hydrofacies types *St,m1*; *St,m2*; *St,f* at 4 m $\leq z \leq$ 5.8 m.

The additional information delivered from the lateral sections A–C and A′–C′ (Fig. 4d) proved to reduce the uncertainties related to the spatial distribution of the litho- and hydrofacies. For instance, a thin layer of the hydrofacies types *Sh/Sp,m1* occurs in each cross-section at $x = 26$ m and $z = 3$ m (Fig. 4a–c). Intuitively, it could be assumed that this layer is laterally continuous through all sections based on the information from the three main cross-sections. Only with the lateral section could it be observed that this layer is discontinuous, pinches out and reappears in section B–B′ as demonstrated in the lateral cross-section E–E′ in Fig. 2c.

The average hydraulic conductivity and porosity of the aquifer analog, using a geometric mean, result in $K = 1.36 \times 10^{-4}$ m/s $\pm$ 3.83×10^{-4} and $n = 0.29 \pm 0.03$. The average values are calculated based on the areal percentage of the hydrofacies types for all cross-sections. The range of hydraulic conductivity varies over five orders of magnitude from $K = 1.38 \times 10^{-3}$–7.84×10^{-8} m/s within the examined deposits (Table 1; Fig. 5). Considering the layered heterogeneity of the system and the high degree of connectivity of the hydrofacies, it can be assumed that the integral hydraulic conductivity for a horizontal flow regime is best approximated by the arithmetic mean with $K = 2.74 \times 10^{-4}$ m/s. An important fact has to be regarded for the highly conductive portions (hydrofacies *Sh/Sp,m1*: $K = 1.38 \times 10^{-3}$ m/s) of the aquifer analog in terms contaminant transport. Conductivity contrasts with high permeable zones in heterogeneous porous media cause groundwater streamlines to converge and diverge, resulting in flow focusing and enhanced transverse mixing and reaction (Werth et al. 2006). For vertical flow directions the low permeable units of the trough cross bedded fine sands (*St,f*: $K = 6.23 \times 10^{-6}$ m/s) on top are more relevant for the system. The minor presence of the clay fragments (*Fm*: $K = 7.84 \times 10^{-8}$ m/s) of <1 % in the entire outcrop does not play a hydraulically relevant role in the aquifer analog.

Conclusion and discussion

Detailed sedimentological and hydrogeological investigations were conducted in an open pit mine near the city of Descalvado (SP), Brazil, to identify hydraulic properties and spatial hydraulic variations of the heterogeneous fluvial–aeolian deposits in the upper part of the Pirambóia Formation of the GAS. A sand body of the size $Lx = 28$ m, $Ly = 7$ m and $Lz = 5.8$ m was carefully examined and gradually excavated to construct three equally spaced 2D cross-sections following the common aquifer analog construction practice. The existing aquifer analog construction procedure (Bayer et al. 2011) was amended in this study by additionally constructing cross-sections of the corresponding lateral sections of the sandy body as described in Kessler et al. (2012). The assemblage of the three 2D cross-section maps with the corresponding lateral cross-sections considerably reduced the uncertainties related to the three-dimensional shape of identified sedimentary structures. Although the aquifer analog construction process and the chosen discretization scale yield satisfying results, additional lateral sections throughout the outcrop are recommended in future aquifer analog studies, in order to better represent discontinuities and small-scale variations of sedimentary features in the middle of the sedimentary block.

Five lithofacies types were identified and further categorized into nine hydrofacies types providing a detailed insight into the heterogeneity of the fluvial–aeolian facies association in the upper Pirambóia Formation. A quantitative description of spatial hydraulic parameter distribution, based on lithofacies and hydrofacies categories with their spatial

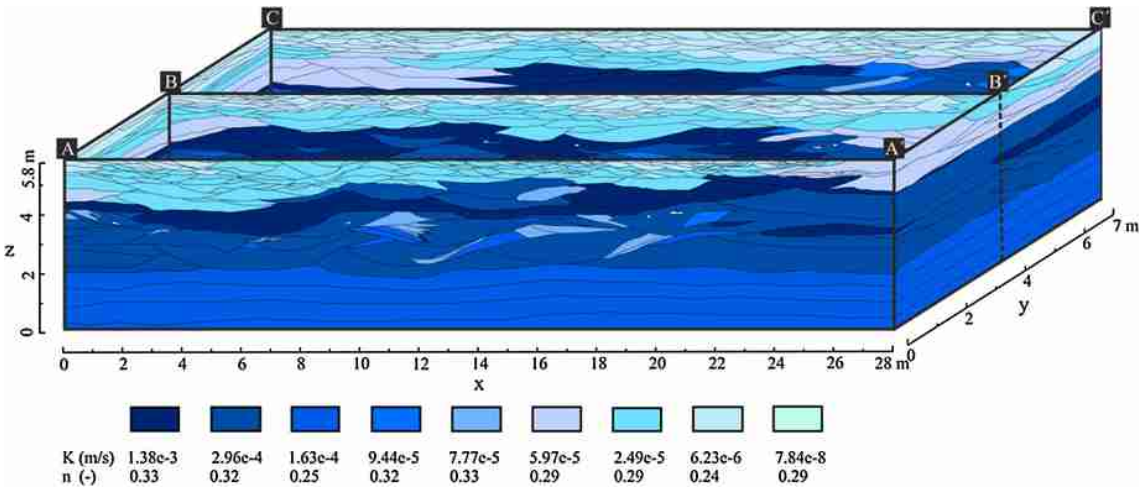

Fig. 5 Hydraulic conductivity (K) and porosity (n) distribution of the quasi-three-dimensional aquifer analog model

distribution and volumetric shares is provided. In combination with modeling tools, the generated dataset allows for the simulation of groundwater pollution scenarios representing realistic field conditions of similar sedimentary settings. Therefore, it serves as a platform to test and evaluate the potential effects of anisotropic flow and contaminant migration patterns as well as the feasibility of the necessary remediation measures on a local scale.

Further, the dataset provides the basis to develop a volumetric 3D model conditioned by the outcrop cross-sections using stochastic methods, as well as numerical up-scaling procedures. For these above mentioned purposes and applications primary geostatistical quantities such as facies specific volumetric fractions, correlation lengths, and anisotropies can be derived. Alternatively, transition probabilities between different facies may be determined or the facies mosaics may serve as training patterns to apply multi-point geostatistics (Comunian et al. 2011).

The following outcomes of this aquifer analog study are considered especially relevant: (1) the horizontally laminated to planar cross-stratified sands could be identified as most the permeable unit within the examined facies association (hydrofacies *Sh/Sp,m1* $= 1.38 \times 10^{-3}$ m/s); (2) the high permeable hydrofacies *Sh/Sp,m1* is relatively well connected throughout the entire outcrop and therefore, can serve as preferential groundwater flow path. If an aquifer with this type of sediments is contaminated a pronounced fingering of a contaminant plume can occur.

Commonly, practitioners see the GAS as a relatively homogeneous system. Existing studies report K estimates for the entire Priambóia Formation in São Paulo State, which range from 3.47×10^{-5} to 5.78×10^{-6} m/s with an average value of 2.89×10^{-5} m/s (Hirata et al. 2011). This data is in concordance with the work of Araújo et al. (1999), which reports an average K of 2.19×10^{-5} m/s for the entire Pirambóia Formation. The Botucatu Formation in São Paulo State has an average hydraulic conductivity of $K = 4.05 \times 10^{-5}$ m/s (range from 2.31×10^{-5} to 4.63×10^{-5} m/s), which is in the same range as reported for the entire Pirambóia Formation (Hirata et al. 2011). The average K value derived in this study for the fluvial–aeolian facies association of the Pirambóia Formation is higher than the reported range of K values of the entire GAS at São Paulo State. A higher hydraulic conductivity implies higher aquifer vulnerability for areas in São Paulo State, where the fluvial–aeolian deposits of the upper part of the Pirambóia Formation crop out or are close to the ground surface. Additionally, the more pronounced hydraulic conductivity contrasts compared to reported values by Hirata et al. (2011) and Araújo et al. (1999) indicate that in case of contamination, this portion of the Pirambóia Formation is more complex to characterize and remediate.

Although the GAS is very extensive in its dimension, the scale of the presented aquifer analog might be considered as pre-ergodic and at an operative scale is only suited for local applications, the provided approach proved to be helpful for the identification of possible relevant hydrostratigraphic units. It gives valuable insight into local scale aquifer heterogeneities of the GAS in the upper Pirambóia Formation, which should also be considered in a regional scale context. The overall thickness of the fluval-aeolian deposits of the upper Pirambóia Formation ranges from only a few meters to ~45 m (Caetano-Chang and Wu 2006). In contrast to the overall thickness of the GAS units in São Paulo State (Pirambóia Formation: 75–270 m, Botucatu Formation: 20–238 m (Hirata et al. 2011)), the examined deposits might seem of subordinated importance. However, considering the pollution threats of the GAS in the São Paulo State, it must be pointed out that only detailed hydraulic information of all hydrostratigraphic units, even if they are thin, allows the recognition of potential contaminant flow pathways, which is necessary for reliable mass flux calculations to assess down gradient risks (ITRC 2010). This is particularly true for highly permeable aquifer units, e.g. the fluvial–aeolian sediments examined in this study.

The detailed characterization of parts of the reservoir helps to improve the understanding of the entire GAS. In particular, the findings aid conceptual model development of aquifer segments where little or no site-specific data are available or for confined areas. Eventually, the work should initialize and foster the construction of additional aquifer analogs of other stratigraphic units of the GAS, to contribute to an advanced reservoir understanding and to support local and regional groundwater management policies.

Acknowledgments We are grateful to Noedir Nava from Mineraçao Jundu for the excellent collaboration and for the equipment provided during the fieldwork in Descalvado. The German Federal Ministry for Education and Research (BMBF) scholarship program for International Postgraduate Studies in Water Technologies (IPSWaT) funds this research and is highly acknowledged. We also thank the three anonymous reviewers for their helpful comments and suggestions.

References

ABGE (Brazilian Association of Geology and Engineering) (1981) Ensaios de Permeabilidade em Solos : orientações para a sua execução no campo–1[a], vol 4. Associação brasileira de geologica de engenharia, São Paulo

Anderson MP (1989) Hydrogeologic facies models to delineate large-scale spatial trends in glacial and glaciofluvial sediments. Geol Soc Am Bull 101(4):501–511

Anderson MP, Aiken JS, Webb EK, Mickelson DM (1999) Sedimentology and hydrogeology of two braided stream deposits. Sediment Geol 129(3–4):187–199. doi:10.1016/s0037-0738(99)00015-9

Araújo LM, França AB, Potter PE (1999) Hydrogeology of the Mercosul aquifer system in the Paraná and Chaco-Paraná Basins, South America, and comparison with the Navajo-Nugget aquifer system, USA. Hydrogeol J 7:317–336. doi:10.1007/s100400050205

Assine ML, Piranha JM, Carneiro CDR (2004) Os paleodesertos Pirambóia e Botucatu. In: Mantesso-Neto V, Batorelli A, Carneiro CDR, Brito-Neves BB (eds) Geologia do Continente Sul-Americano: Evolução da obra de Fernando Flávio Marques de Almeida. Editora Beca, São Paulo, pp 77–92

Bayer P, Huggenberger P, Renard P, Comunian A (2011) Three-dimensional high resolution fluvio-glacial aquifer analog: Part 1: field study. J Hydrol 405(1–2):1–9. doi:10.1016/j.jhydrol.2011.03.038

Bersezio R (2007) Aquifer Analogues. Mem Descr Carta Geol d'It:39–50

Bersezio R, Bini A, Giudici M (1999) Effects of sedimentary heterogeneity on groundwater flow in a Quaternary pro-glacial delta environment: joining facies analysis and numerical modelling. Sediment Geol 129(3–4):327–344. doi:10.1016/s0037-0738(98)00145-6

Bersezio R, Pavia F, Baio M, Bini A, Felletti F, Rodondi C (2004) Aquifer architecture of the Quaternary alluvial succession of the southern lambro basin (Lombardy-Italy). Quaternario 17(2/1):361–378

Bersezio R, Felletti F, Giudici M, Miceli A, Zembo I (2007) Aquifer analogues to assist modeling of groundwater flow: the Pleistocene aquifer complex of the Agri Valley (Basilicata). Mem Descr Carta Geol d'It:51–66

Bonotto D (2012) A comparative study of aquifer systems occurring at the Paraná sedimentary basin, Brazil: major hydrochemical trends. Environ Earth Sci 67(8):2285–2300. doi:10.1007/s12665-012-1676-1

Bonotto DM (2013) A comparative study of aquifer systems occurring at the Paraná sedimentary basin, Brazil: U-isotopes contribution. Environ Earth Sci 68(5):1405–1418. doi:10.1007/s12665-012-1838-1

Caetano-Chang MR, Wu FT (2006) Arenitos flúvio-eólicos da porção superior da Formação Pirambóia no centro-leste paulista. Rev Bras Geociências 36(2):296–304

Cardenas MB, Zlotnik VA (2003) Three-dimensional model of modern channel bend deposits. Water Resour Res 39(6):1141. doi:10.1029/2002wr001383

Carrier WD (2003) Goodbye, Hazen; Hello, Kozeny–Carman. J Geotech Geoenviron 129(11):1054–1056. doi:10.1061/(asce)1090-0241(2003)129:11(1054)

Comunian A, Renard P, Straubhaar J, Bayer P (2011) Three-dimensional high resolution fluvio-glacial aquifer analog—Part 2: Geostatistical modeling. J Hydrol 405(1–2):10–23. doi:10.1016/j.jhydrol.2011.03.037

DAEE (São Paulo State Water and Electricity Department.); IG (Geology Department São Paulo State), IPT (Institute for Research and Technology); CPRM (Geological Survey of Brazil) (2005) Mapa de Águas Subterrâneas do Estado de São Paulo. São Paulo

Dantas AD, Paschoalato CFR, Martinez MS, Ballejo RR, Di Bernardo L (2011) Removal of diuron and hexazinone from Guarany aquifer groundwater. Braz J Chem Eng 28(3):415–424. doi:10.1590/S0104-66322011000300007

Dias KDN, Scherer CMS (2008) Cross-bedding set thickness and stratigraphic architecture of aeolian systems: an example from the Upper Permian Pirambóia Formation (Paraná Basin), southern Brazil. J S Am Earth Sci 25(3):405–415. doi:10.1016/j.jsames.2007.07.008

DIN EN ISO 14688-1 (2002) Geotechnical Investigation and testing—identification and classification of soil—Part 1: Identification and description (ISO 14688-1:2002); German version EN ISO 14688-1:2002

Donatti LM, Sawakuchi AO, Giannini PCF, Fernandes LA (2001) The Pirambóia-Botucatu Succession (Late Permian—Early Cretaceous, Paraná basin, São Paulo and Paraná states): two contrasting eaolian systems. An Acad Bras Cienc 73(3):465

Felletti F, Bersezio R, Giudici M (2006) Geostatistical simulation and numerical upscaling, to model ground-water flow in a sandy-gravel, braided river, aquifer analogue. J Sediment Res 76(11–12):1215–1229. doi:10.2110/jsr.2006.091

Fetter CW (2001) Applied Hydrogeology, 4th edn. Prentice-Hall, Inc., New Jersey

Flint SS, Bryant ID (1993) Quantitative clastic reservoir geological modelling; problems and perspectives. The geological modelling of hydrocarbon reservoirs and outcrop analogues. Special Publ Int Assoc Sedimentol 15:3–20

Foster S, Hirata R, Vidal A, Schmidt G, Garduño H (2009) The Guaraní aquifer initiative—towards realistic groundwater management in a transboundary context, GW-MATE (The Groundwater Management Advisory Team) case profile collection No. 9; The World Bank. http://siteresourcesworldbankorg/INTWAT/Resources/GWMATE_English_CP_09pdf. Accessed 4th October 2012

Gastmans D, Veroslavsky G, Kiang Chang H, Caetano-Chang MR, Nogueira Pressinott MM (2012) Modelo hidrogeológico conceptual del Sistema Acuífero Guaraní (SAG): una herramienta para la gestión. Boletín Geológico y Minero 123(3):249–265

Goldemberg J, Coelho ST, Guardabassi P (2008) The sustainability of ethanol production from sugarcane. Energ Policy 36(6):2086–2097. doi:10.1016/j.enpol.2008.02.028

Grathwohl P, Rügner H, Wöhling T, Osenbrück K, Schwientek M, Gayler S, Wollschläger U, Selle B, Pause M, Delfs J-O, Grzeschik M, Weller U, Ivanov M, Cirpka O, Maier U, Kuch B, Nowak W, Wulfmeyer V, Warrach-Sagi K, Streck T, Attinger S, Bilke L, Dietrich P, Fleckenstein J, Kalbacher T, Kolditz O, Rink K, Samaniego L, Vogel H-J, Werban U, Teutsch G (2013) Catchments as reactors: a comprehensive approach for water fluxes and solute turnover. Environ Earth Sci 69(2):317–333. doi:10.1007/s12665-013-2281-7

Heinz J, Aigner T (2003) Hierarchical dynamic stratigraphy in various Quaternary gravel deposits, Rhine glacier area (SW Germany): implications for hydrostratigraphy. Int J Earth Sci 92:923–938. doi:10.1007/s00531-003-0359-2

Heinz J, Kleineidam S, Teutsch G, Aigner T (2003) Heterogeneity patterns of Quaternary glaciofluvial gravel bodies (SW-Germany): application to hydrogeology. Sediment Geol 158(1–2):1–23. doi:10.1016/s0037-0738(02)00239-7

Hirata R, Gesicki A, Sracek O, Bertolo R, Giannini PC, Aravena R (2011) Relation between sedimentary framework and hydrogeology in the Guarani Aquifer System in São Paulo state, Brazil. J S Am Earth Sci 31(4):444–456. doi:10.1016/j.jsames.2011.03.006

Hornung J, Aigner T (1999) Reservoir and aquifer characterization of fluvial architectural elements: Stubensandstein, Upper Triassic, southwest Germany. Sediment Geol 129(3–4):215–280. doi:10.1016/S0037-0738(99)00103-7

Huggenberger P, Aigner T (1999) Introduction to the special issue on aquifer-sedimentology: problems, perspectives and modern approaches. Sed Geol 129(3–4):179–186. doi:10.1016/s0037-0738(99)00101-3

ITRC (2010) Use and measurement of mass flux and mass discharge. Interstate Technology & Regulatory Council, Washington, DC, Integrated DNAPL Site Strategy Team

Kasenow M (2002) Determination of hydraulic conductivity from grain size analysis. Water Resources Publications, Littleton

Kessler TC, Comunian A, Oriani F, Renard P, Nilsson B, Klint KE, Bjerg PL (2012) Modeling fine-scale geological heterogeneity—

examples of sand lenses in Tills. Ground Water. doi:10.1111/j.1745-6584.2012.01015.x

Klingbeil R, Kleineidam S, Asprion U, Aigner T, Teutsch G (1999) Relating lithofacies to hydrofacies: outcrop-based hydrogeological characterisation of Quaternary gravel deposits. Sediment Geol 129(3–4):299–310. doi:10.1016/s0037-0738(99)00067-6

Koltermann CE, Gorelick SM (1996) Heterogeneity in sedimentary deposits: a review of structure-imitating, process-imitating, and descriptive approaches. Water Resour Res 32(9):2617–2658. doi:10.1029/96wr00025

Kostic B, Becht A, Aigner T (2005) 3-D sedimentary architecture of a Quaternary gravel delta (SW-Germany): implications for hydrostratigraphy. Sediment Geol 181(3–4):147–171. doi:10.1016/j.sedgeo.2005.07.004

Lago A, Elis V, Borges W, Penner G (2009) Geophysical investigation using resistivity and GPR methods: a case study of a lubricant oil waste disposal area in the city of Ribeirão Preto, São Paulo, Brazil. Environ Geol 58(2):407–417. doi:10.1007/s00254-008-1511-x

Marimon M, Roisenberg A, Viero A, Oliveira Camargo F, Suhogusoff A (2013) Evaluation of the potential impact of fluorine-rich fertilizers on the Guarani Aquifer System, Rio Grande do Sul, Southern Brazil. Environ Earth Sci 69(1):77–84. doi:10.1007/s12665-012-1935-1

Miall AD (1978) Fluvial sedimentology. In: Miall AD (ed) Lithofacies types and vertical profile models in braided river deposits: a summary. Mem. Can Soc Petrol Geol, pp 597–604

Miall AD (2010) The geology of fluvial deposits: sedimentary facies, basin analysis, and petroleum geology. Springer, Berlin

Milani EJ, Faccini UF, Scherer CM, Araujo LM, Cupertino JA (1998) Sequences and stratigraphic hierarchy of the Paraná basin (Ordovician to Cretaceous), Southern Brazil, Boletim IG USP. Série Científica 29:126–173

Morales N, D'Affonseca FM, Perinotto JAJ (1997) Utilização de ortofotografia terrestre em geologia, exemplificada pelo estudo de afloramentos da formação Tatuí. VII Simpósio de quantificação em geociências, Rio Claro (SP)

Oliveira EG (2000) Hidrogeoquímica aplicada na avaliação do impacto ambiental em áreas de lavra de areia. PhD Thesis, University of São Paulo State (UNESP), Rio Claro

Parker BL, Chapman SW, Guilbeault MA (2008) Plume persistence caused by back diffusion from thin clay layers in a sand aquifer following TCE source-zone hydraulic isolation. J Contam Hydrol 102(1–2):86–104. doi:10.1016/j.jconhyd.2008.07.003

Poeter E, Gaylord DR (1990) Influence of aquifer heterogeneity on contaminant transport at the Hanford site. Ground Water 28(6):900–909. doi:10.1111/j.1745-6584.1990.tb01726.x

Pringle JK, Howell JA, Hodgetts D, Westerman AR, Hodgson DM (2006) Virtual outcrop models of petroleum reservoir analogues: a review of the current state-of-the-art. First Break 24:33–42

Puri S, Appelgren B, Arnold G, Aureli A, Burchi S, Burke J, Margat J, Pallas P (2001) Internationally shared (transboundary) aquifer resources management, their significance and sustainable management: a framework document. IHP-VI, Int Hydrol Program, Non Ser Publ Hydrol 40. UNESCO, Paris

Rabelo J, Wendland E (2009) Assessment of groundwater recharge and water fluxes of the Guarani Aquifer System, Brazil. Hydrogeol J 17(7):1733–1748. doi:10.1007/s10040-009-0462-y

Schmidt G, Vassolo S (2011) Untersuchungen zu einem der größten Grundwasservorkommen Südamerikas: Der Guaraní-Aquifer in Paraguay. Grundwasser 16(3):187–194. doi:10.1007/s00767-011-0171-z

Soares AP, Soares PC, Holz M (2008) Heterogeneidades hidroestratigráficas no Sistema Aqüífero Guarani. Rev Bras Geociências 38(4):598–617

Sweet ML, Blewden CJ, Carter AM, Mills CA (1996) Modeling heterogeneity in a low-permeability gas reservoir using geostatistical techniques, Hyde field, southern North Sea. AAPG Bull 80(11):1719–1735

Vukovic M, Soro A (1992) Determination of hydraulic conductivity of porous media from grain-size composition. Water Resources Publications, Littleton

Weissmann GS, Carle SF, Fogg GE (1999) Three-dimensional hydrofacies modeling based on soil surveys and transition probability geostatistics. Water Resour Res 35(6):1761–1770. doi:10.1029/1999wr900048

Wendland E, Barreto C, Gomes LH (2007) Water balance in the Guarani Aquifer outcrop zone based on hydrogeologic monitoring. J Hydrol 342(3–4):261–269. doi:10.1016/j.jhydrol.2007.05.033

Werth CJ, Cirpka OA, Grathwohl P (2006) Enhanced mixing and reaction through flow focusing in heterogeneous porous media. Water Resour Res 42(12):W12414. doi:10.1029/2005wr004511

Whittaker J, Teutsch G (1999) Numerical simulation of subsurface characterization methods: application to a natural aquifer analogue. Adv Water Resour 22(8):819–829. doi:10.1016/s0309-1708(98)00056-6

Zappa G, Bersezio R, Felletti F, Giudici M (2006) Modeling heterogeneity of gravel-sand, braided stream, alluvial aquifers at the facies scale. J Hydrol 325(1–4):134–153. doi:10.1016/j.jhydrol.2005.10.016

Zuquette L, Palma J, Pejon O (2009) Methodology to assess groundwater pollution conditions (current and pre-disposition) in the São Carlos and Ribeirão Preto regions, Brazil. B Eng Geol Environ 68(1):117–136. doi:10.1007/s10064-008-0173-y